Determination of the plane wave modulus of a poroelastic solid saturated by a 2-phase fluid using harmonic experiments.

Juan E. Santos [a,b,*] Gabriela B. Savioli [a]

[a] *Universidad de Buenos Aires, Facultad de Ingenieria, Instituto del Gas y del Petróleo, Av. Las Heras 2214, Piso 3, CABA, Argentina*

[b] *Department of Mathematics, Purdue University, 150 N. University Street, West Lafayette, Indiana, 47907-2067, USA; santos@math.purdue.edu*

* Corresponding author, e-mail: santos@math.purdue.edu

Preprint submitted to Comput. Methods Appl. Mech. Engrg. 13 November 2017

Abstract

An effective viscoelastic medium is derived using harmonic FE numerical experiments in a poroelastic solid saturated by a 2-phase fluid.

Key words: , Poroviscoelasticity, Finite element methods, Effective viscoleastic media

1 Numerical experiments

1.1 validation of the procedure

To validate the proposed methodology, we performed the compressibility test to determine the P-wave phase velocities and attenuation coefficients for the case in which the sample is a periodic media consisting of alternating layers of equal thickness 0.1 m with saturated with a two-phase fluid, chosen to be gas and water, with total gas saturation 50 %. Residual saturations are $S_{rn} = S_{rw}$ =0.001 and saturation values are $S_n = 0.012$ in the first layer and $S_n = 0.988$ in the second layer. In this fashion, we have almost full water saturation in the first layer and almost full gas saturation in the second layer. Here and in all experiments capillary pressure amplitude A is 30 kPa. The results are compared with those of the White model and the harmonic compressibility test as described in [**?**] for single-phase fluids. For this purpose we constructed an effective single-phase fluid weighting the gas and water properties with the corresponding saturations on each layer. The mesh size is 60× 60 for both the two-phase and single-phase models.

Figures 1 and 2 compares phase velocities and attenuation coefficients as function of frequency in the range 1 Hz-300 Hz with those of the White model and the harmonic compressibility test as described in [**?**] for single-phase fluids. For this purpose we constructed an effective single-phase fluid weighting the gas and water properties with the corresponding saturations on each layer. The mesh size is 60× 60 for both the two-phase and single-phase models.

Besides, for the White model, we consider a periodic medium composed of alternating layers but of equal thickness 0.2 m saturated with the effective fluid. This comparison is valid because the boundary conditions (**??**)-(**??**) for the compressibility test can be associated with a compression similar to that proposed by [**?**], but applied to a periodic sample obtained by a mirror reflection with respect to the x-axis of the domain Ω.

The physical properties of the solid matrix are taken constant in all the domain, and correspond to the Sandstone 1 in Table 1, while the physical properties of the fluids (water and gas) are given in Table 2.

As can be observed in Figures 1 and 2, while velocities and attenuation coefficients for the SFBM are in very good agreement with those predicted by White's theory. On the other hand, the case of the 2FBM shows slightly higher attenuation for all frequencies, with the attenuation peak located approximately at the same frequency for the 3 models. Furthermore, phase velocites for the two-phase model show small differences only at low frecuencies.

	Sandstone 1	**Sandstone 2**	**Shale**
K_s	37 GPa	37 GPa	25 GPa
ρ_s	2650 Kg/m^3	2650 Kg/m^3	2550 Kg/m^3
ϕ	0.3	0.2	0.3
K_m	4.8 GPa	12.1 GPa	3.3 GPa
μ	5.7 GPa	14.4 GPa	1.2 GPa
κ	1 Darcy	0.23 Darcy	1.5×10^{-5} Darcy

Table 1. Physical properties of the solid materials used in the numerical examples.

	Water	**Gas**
K_f	2.25 GPa	0.012 GPa
ρ_f	1040 Kg/m^3	78 Kg/m^3
η	0.003Pa·s	0.00015 Pa·s

Table 2. Physical properties of the fluids used in the numerical examples.

The second experiment compares velocities and attenuation coefficients of the White model of periodic layers with those of the two-phase model for the cases of total 10 % and 50 % gas saturation. For both cases the sample and mesh size are the same than in the first experiment.

For the 10 % gas saturation case, the White model considers layers of 4 cm

and 36 cm size with gas saturations 0.012 and 0.988, respectively, while the two-phase model is run for 2cm and 18 cm layers with the same gas saturations of the White model.

While in Figure 3 phase velocities for the two-phase model display only small differences with respect to the White model, Figure 4 shows that attenuation is always stronger for the two-phase model than for the White model. This effect is more noticeable in the 10 % gas saturation case where Q takes the value 27 at about 10 Hz for the White model and 21 at 8 Hz for the two-phase model, i.e., the atenuation peak is shifted to lower frequencies.

1.2 The patchy gas-water saturation case

Patchy gas-water saturation arises in hydrocarbon reservoirs, where regions of non-uniform patchy saturation occur at gas-water contacts. Patchy-saturation patterns produce very important mesoscopic effects at the seismic band of frequencies, as shown by White in [**?**].

In these experiments we consider a square sample of side length 80 cm saturated with a two-phase gas-water fluid spatially distributed in the form of irregular patches. Mesh size is 80×80. The compressibility test was applied for 21 frequencies in the range 1 Hz- 300 Hz. The properties of gas and water are those given in Table 2.

The generations of patchy gas-water distributions was explained in detail in [**?**] for the case of binary fractal distributions and single phase fluids. Here we used a generalization of this procedure to the case of a ternary distribution and two-phase fluids. In this fashion we obtain a ternary fractal patchy two-phase gas-water distribution as in Figure 5.

Figures 6-7 display phase velocities for the SFBM and 2FBM for 6 % and 12 % full gas saturation as function of frequency. It is observed that phase velocities for the SFBM are slightly higher than for the 2FBM at low frequencies and tend to coincide at higher frquencies.

On the other hand, attenuation for the 2FBM is always higher than for the SFBM, and the attenuation peaks for the 2FBM shift to higher frequencies. More precisely, from Figures 6-7 we see that for the SFBM, $Q = 43$ at 30 Hz and $Q = 50$ at 70 Hz, while for the 2FBM $Q = 22$ at 45 Hz and $Q = 30$ at 100 Hz

To illustrate the mesoscopic loss mechanisms, we show the fluid pressure distribution for both the SFBM and 2FBM at 40 Hz and the case of 12 % gas saturation.

For the 2FBM we defined the *fluid pressure* of the two-phase fluid $\widetilde{p}_f$ as

$$\widetilde{\mathrm{p}}_{\mathrm{f}} = \mathcal{T}_n(\mathbf{u}) + \mathcal{T}_w(\mathbf{u}). \tag{1}$$

Figures 8-10 display the fluid pressure distribution at 40 Hz for the SFBM and 2FBM, while Figures 9-11 show the corresponding gradients.

While it is observed that fluid pressures are higher in the 2FBM than for the SFBM, with an increase of about 14 %, to illustrate the mesoscopic loss effect it is more relevant to observe the corresponding gradients, which are more than 10 times higher for the 2FBM than for the SFBM. This clearly explains the highher attenuation effects shown in Figure 7 for the 2FBM as compared with the SFBM.

The next experiment analizes variations on phase velocities and attenuation coefficients fir both the SFBM and 2FBM due to changes in values of correlation lengths, chosen to be CL = 4, 8 and 16 cm. Figure 12 shows that velocities for the 2FBM are always smaller than for the SFBM at low frequencies, and tend to coincide at higher frequencies.

On the other hand, Figure 13 shows that attenuation coefficients are much higher for the 2FBM than for the SFBM, with an increase of about 80 % for all correlation lengths.

Finally we determined the equivalent shear modulus of a highly heterogeneous sample composed of two different materials, shale and sandstone 2 in Table 1, distributed in the form of irregular patches. The two-phase fluid has nonwetting saturation $S_{rn} = 0.0001$ and residual saturations are $S_{ro} = 0, S_{rw} = 0.05$. Thus we have essentially a water saturated sample. Experiments with the SFBM were also run using an effective single phase fluid. Since fluids do not support shear, shear velocities and attenuation coefficients were numerically identical for both models. The comparison curves are not shown for brevity. The generation of the patchy shale-sandstone spatial distribution was performed as explained in [**?**], using stochastic fractal fields of several correlation lengths based in the von Karman spectrum [**?**,**?**].

In this experiments the sample is a square of side length 5 cm. Figure 14 shows a realization for the case correlation length equal to 0.05 cm.

Figure 15 displays shear wave phase velocities for correlation lengths 0.05, 0.0025 and 0.0125 cm as function of frequency, while 16 shows the corresponding attenuation coefficients.

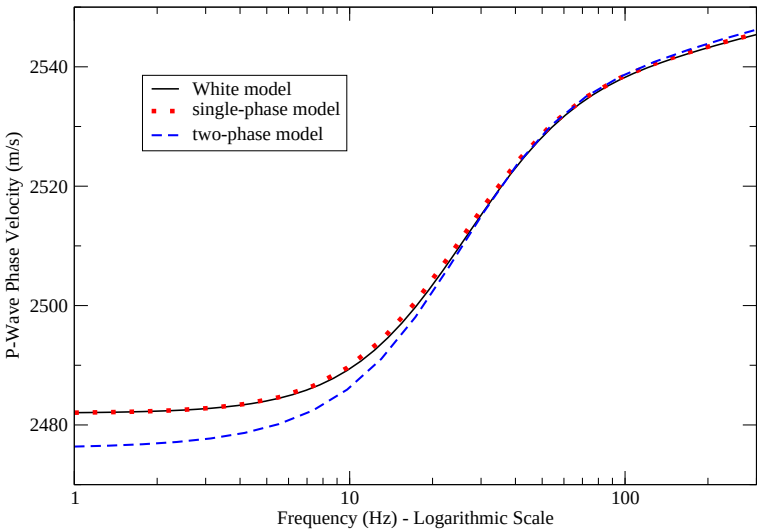

Fig. 1. Validation of P-wave phase velocities by comparison with White model and 1-phase and 2-phase model for capillary pressure amlitude equal to 30 kPa

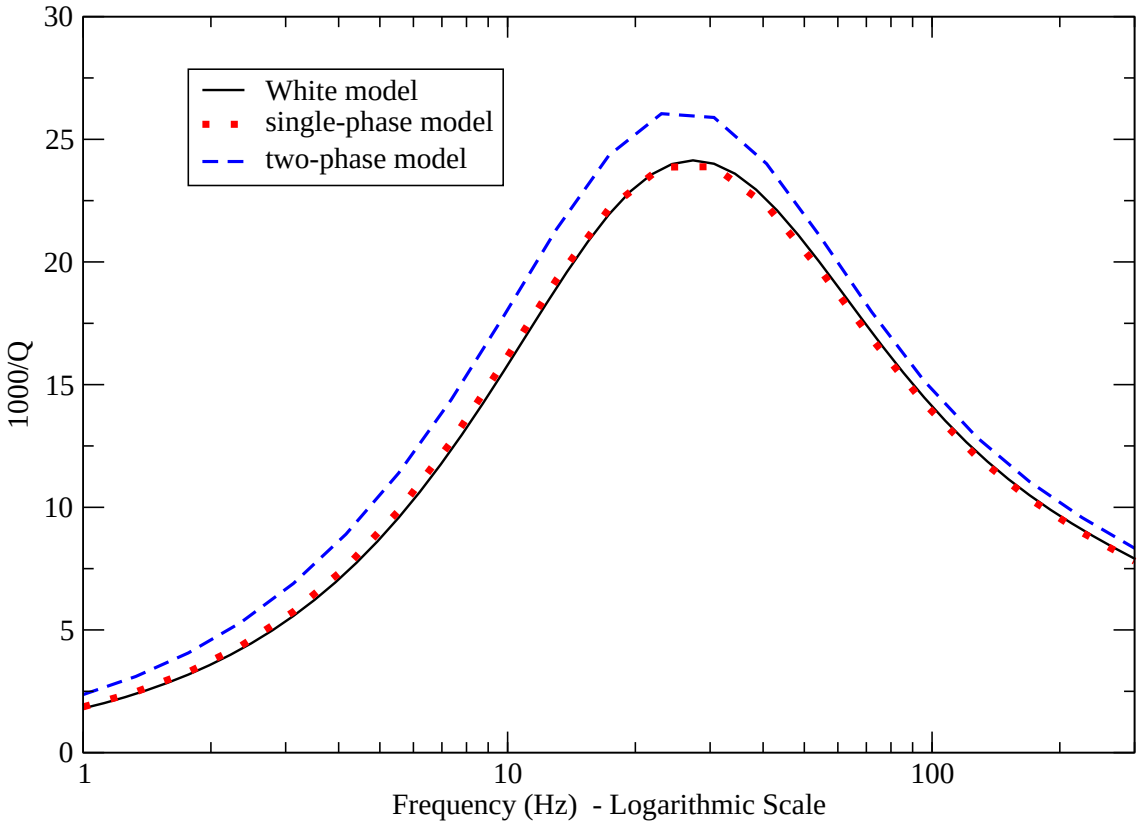

Fig. 2. Validation of dissipation factors by comparison with White model and 1-phase and 2-phase model for capillary pressure amplitude equal to 30 kPa.

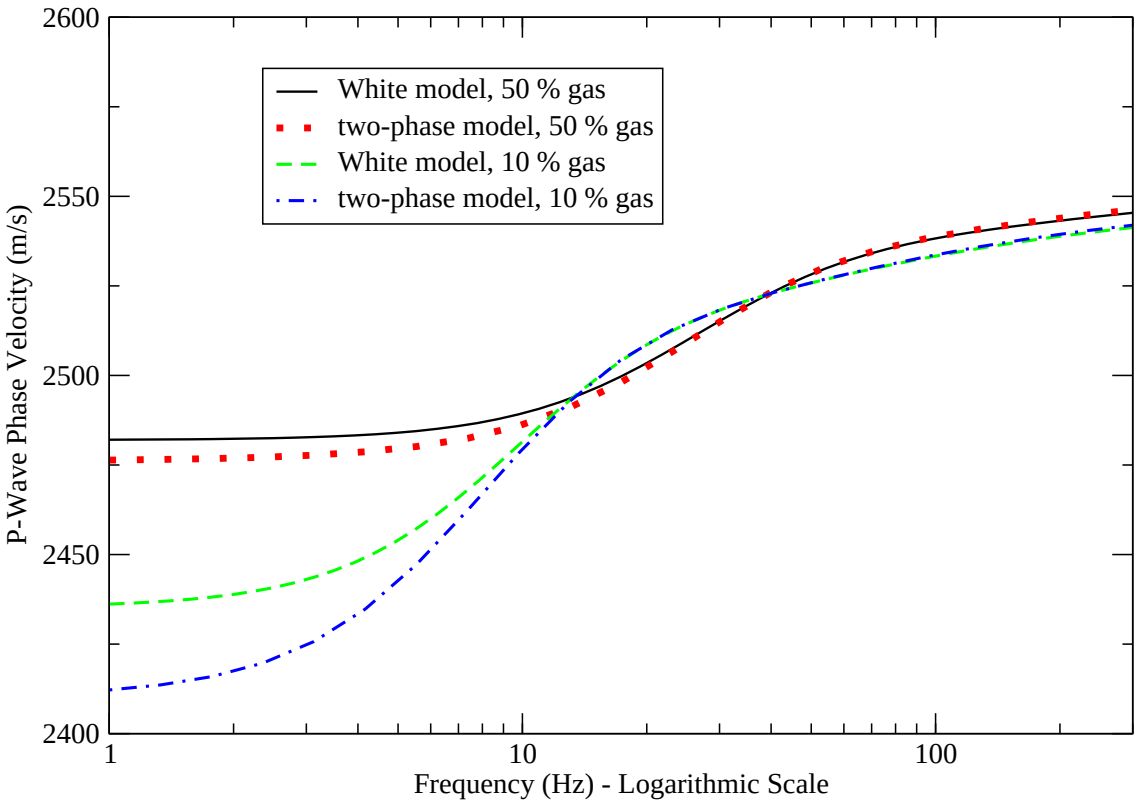

Fig. 3. P-wave phase velocitities for 10 % and 50% full gas saturation.

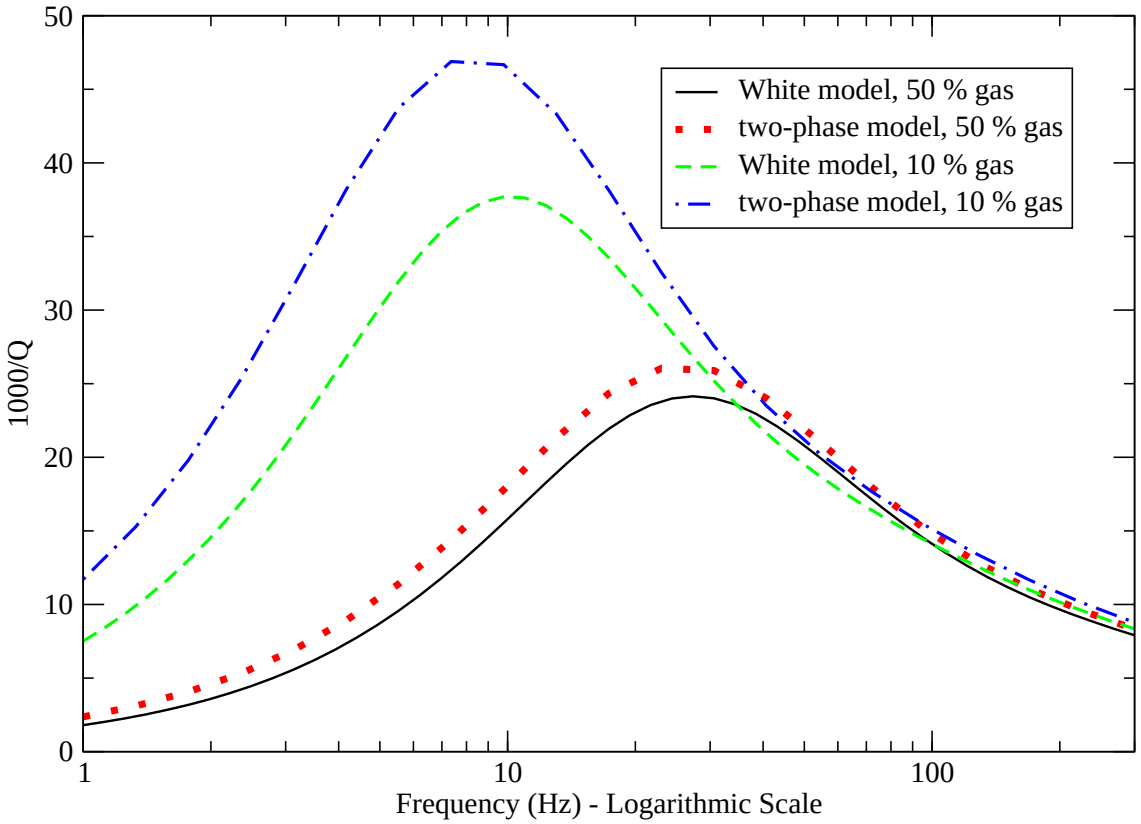

Fig. 4. Dissipation factors for and 10 % and 50% full gas saturation.

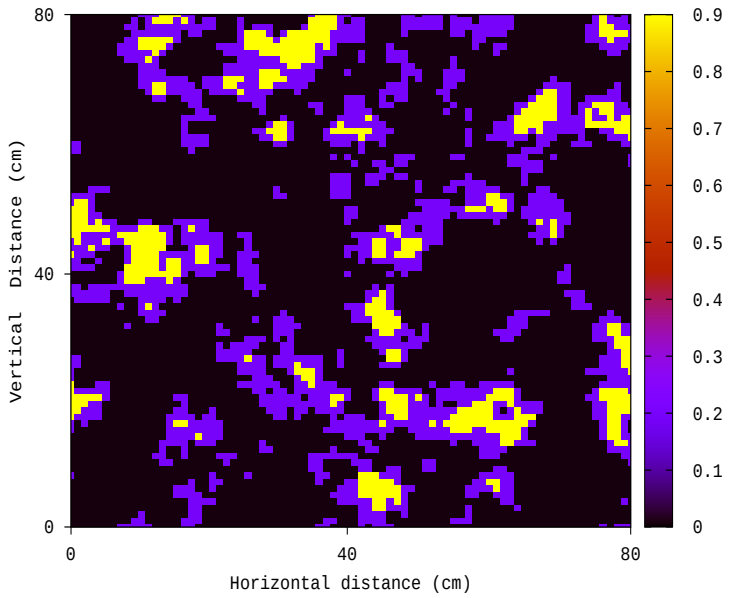

Fig. 5. Patchy distribution of two-phase gas-water distribution. Black zones correspond to $S_n = 0.012$, blue regions to $S_n = 0.2$ and yellow regions to $S_n = 0.898$. The overall gas saturation is 12 %

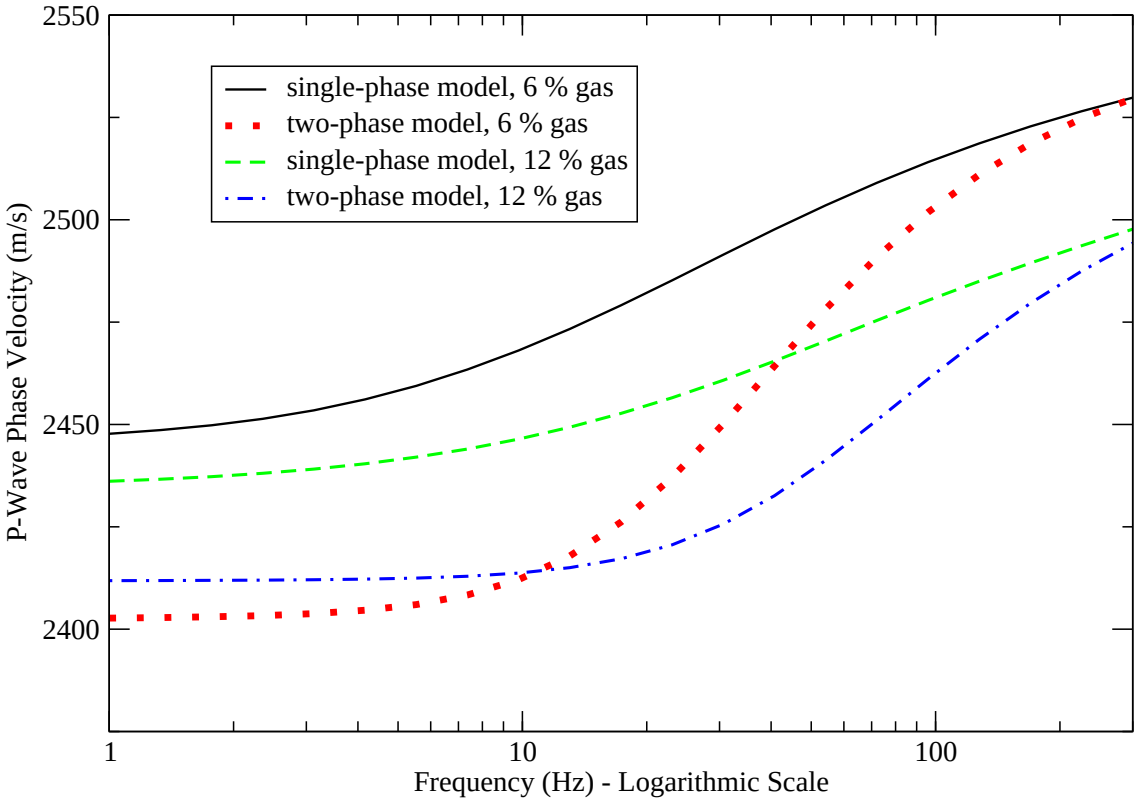

Fig. 6. P-wave phase velocities as function of frequency for single-phase and 2-phase models and 6 % and 12 % gas saturation. Residual saturations are $S_{rn} = 0, S_{rw} = 0.01$

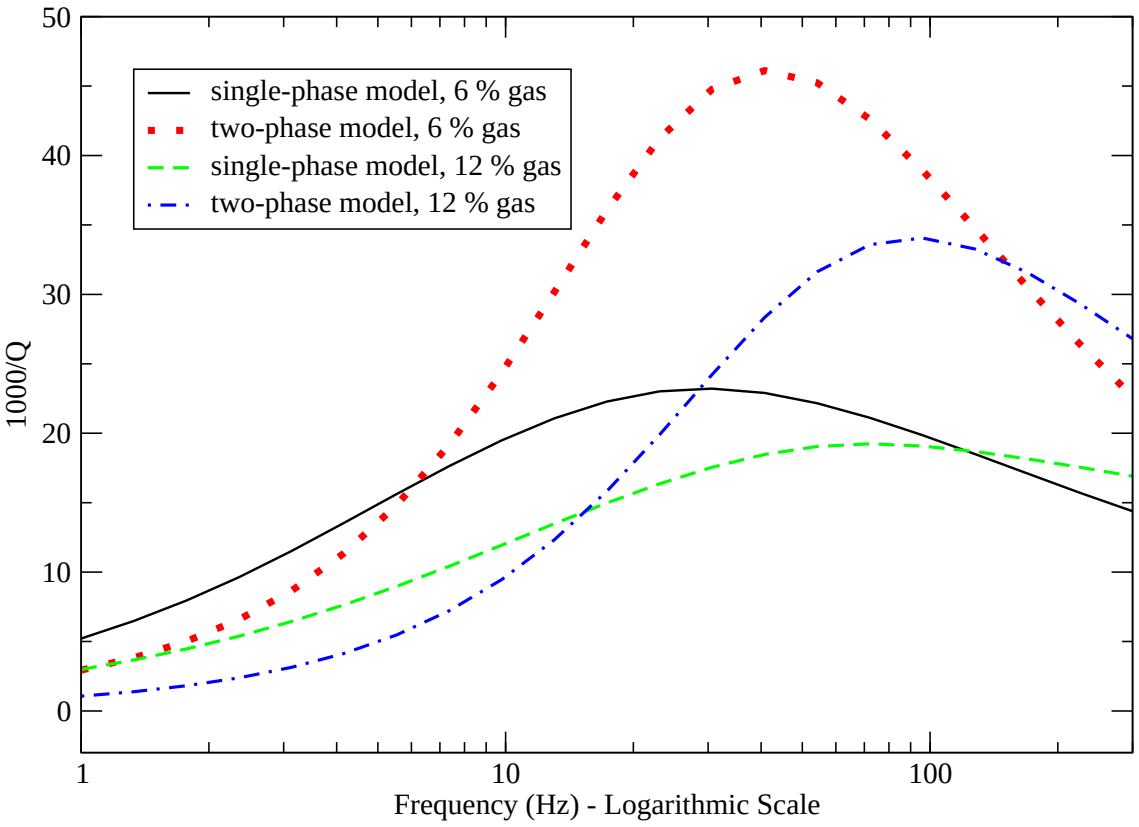

Fig. 7. Dissipation factor as function of frequency for single-phase and 2-phase models and 6 % and 12 % gas saturation. Residual saturations are $S_{rn} = 0, S_{rw} = 0.01$

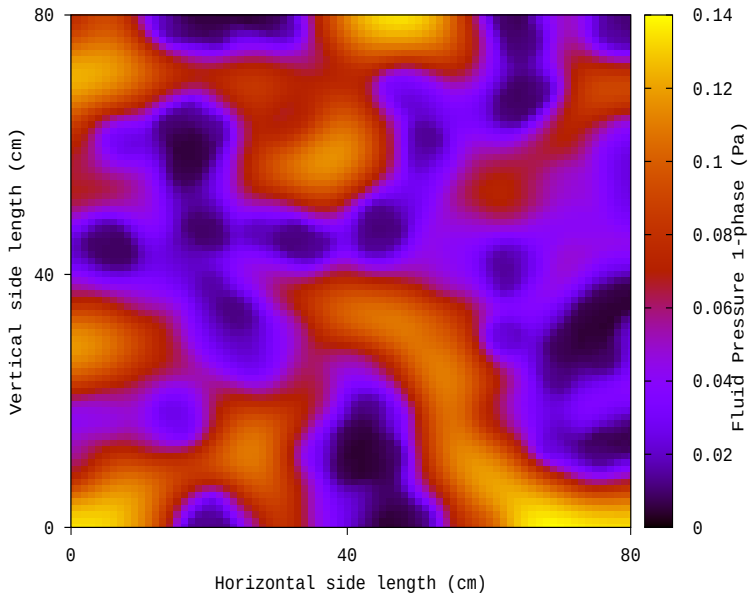

Fig. 8. Fluid pressure for single-phase model at 40 Hz.

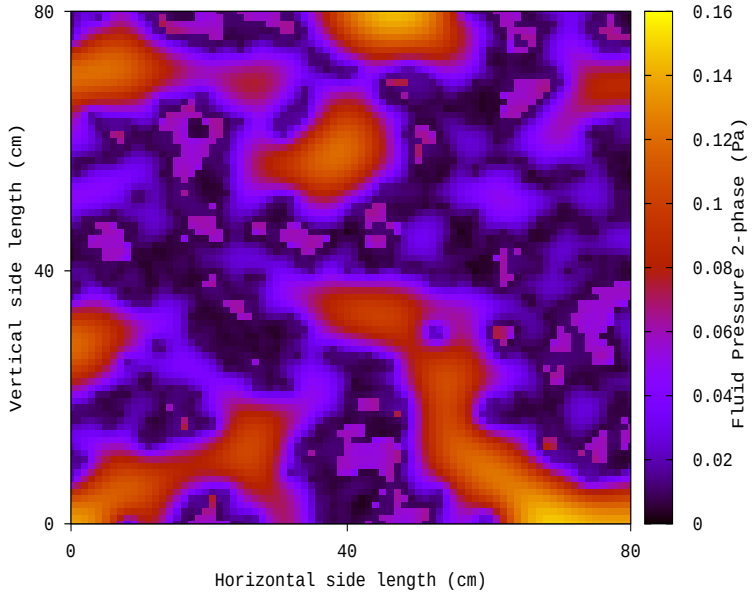

Fig. 9. Fluid pressure for two-phase model at 40 Hz.

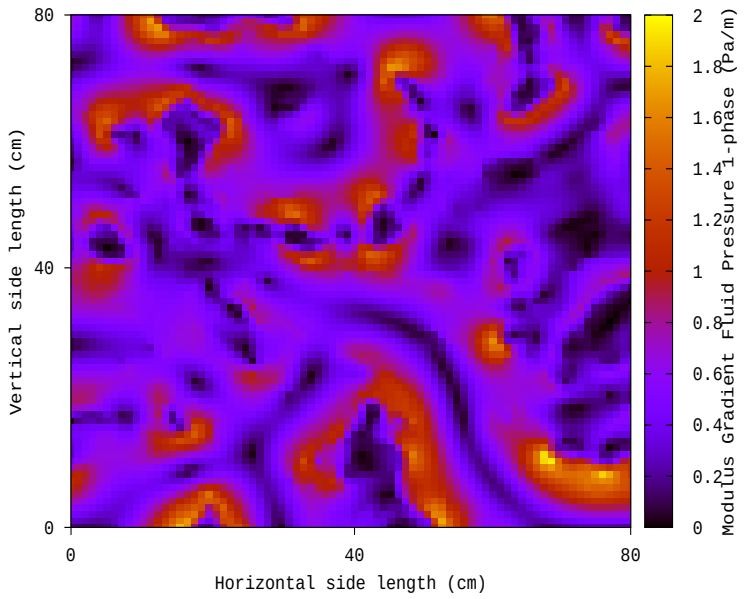

Fig. 10. Modulus of gradient of fluid pressure for single-phase model at 40 Hz.

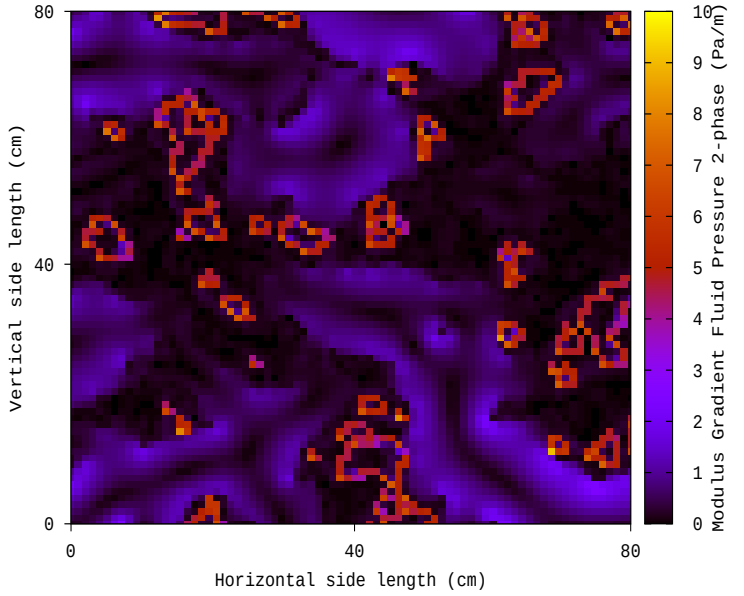

Fig. 11. Modulus of gradient of fluid pressure for two-phase model at 40 Hz.

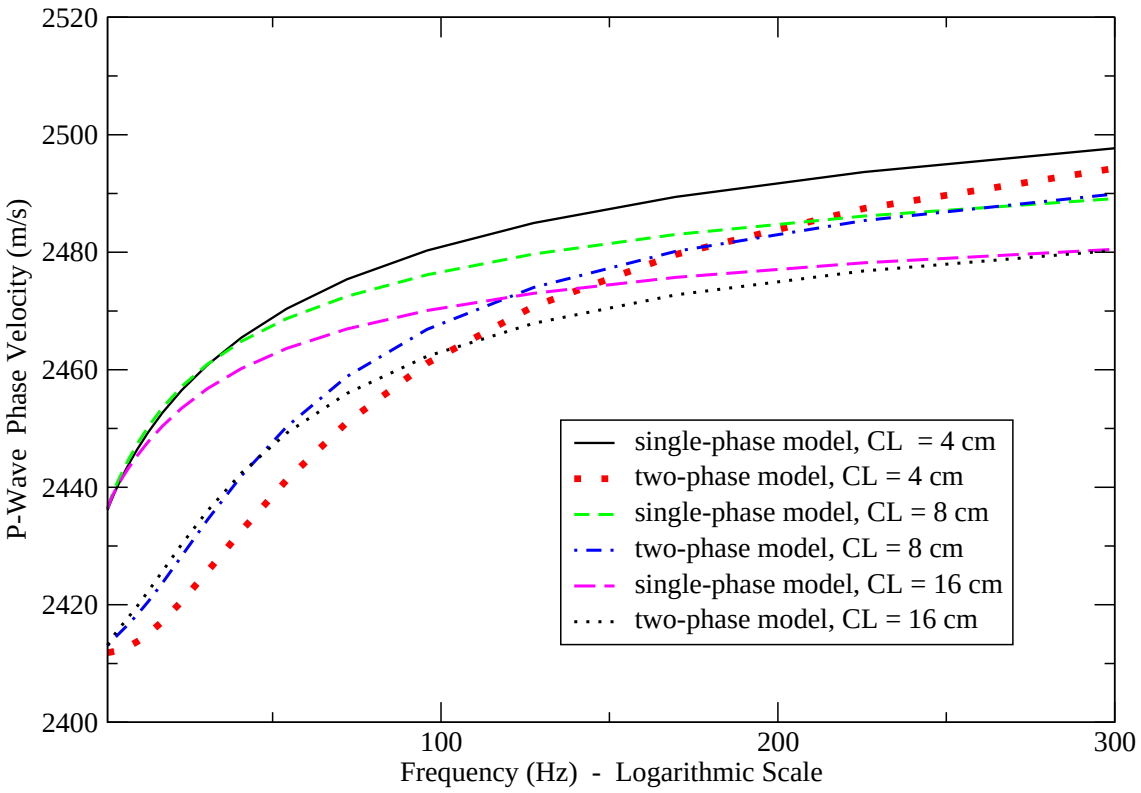

Fig. 12. P-wave phase velocity as function of frequency for single-phase and 2-phase models at 12 % gas saturation at several correlation lengths CL. Residual saturations are $S_{rn} = 0, S_{rw} = 0.1$

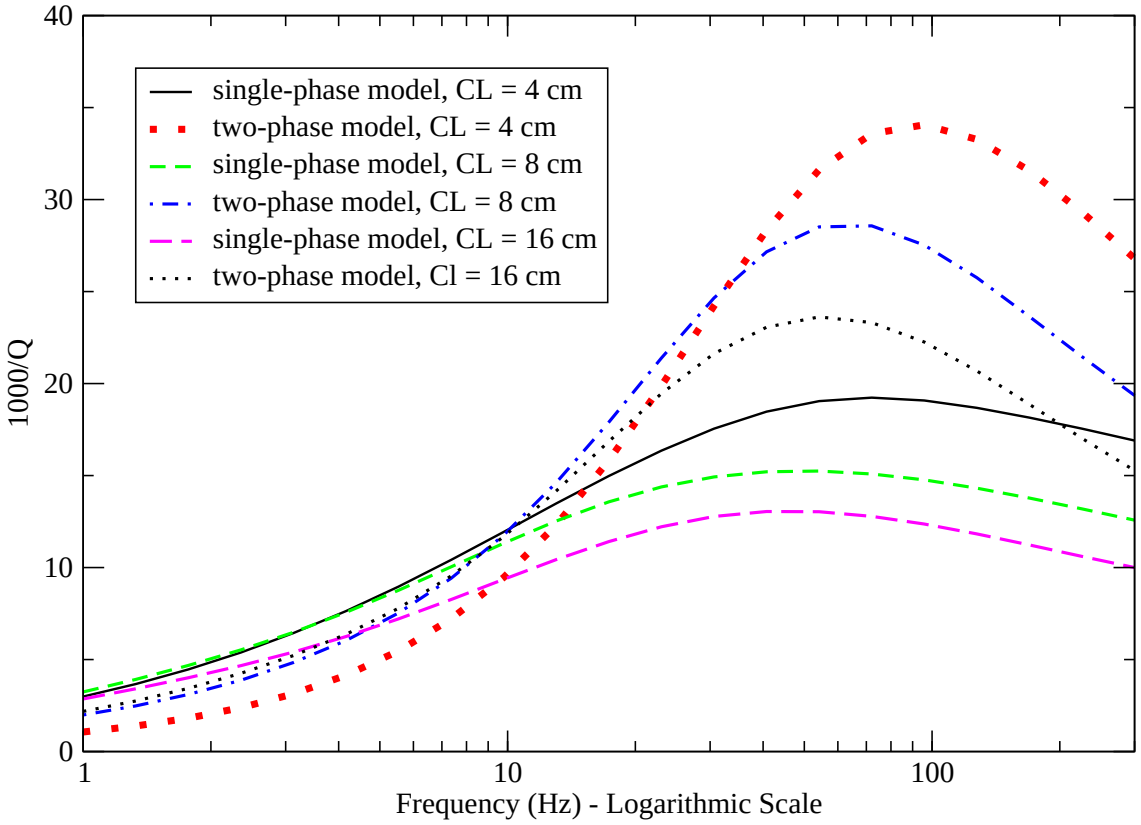

Fig. 13. P-wave attenuation coefficient as function of frequency for single-phase and 2-phase models at 12 % gas saturation at several correlation lengths CL. Residual saturations are $S_{rn} = 0, S_{rw} = 0.1$

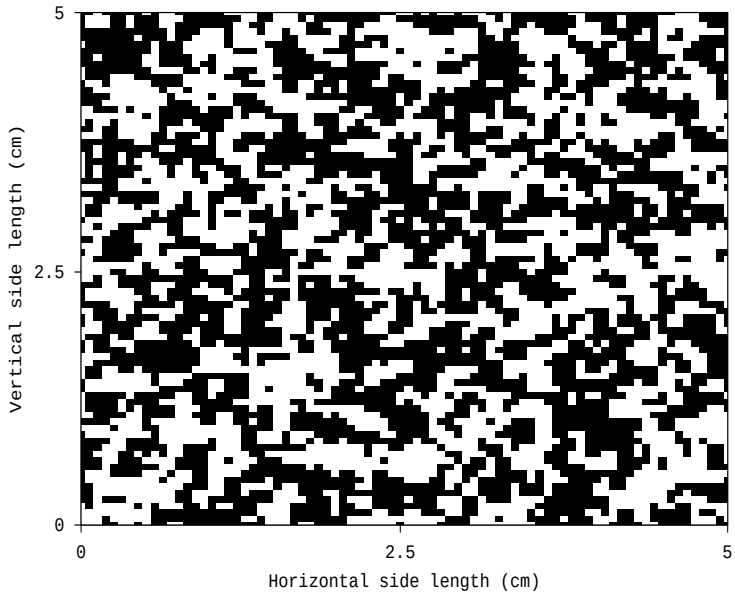

Fig. 14. Fractal shale-sandstone 2 distribution. Black zones correspond to pure shale and white zones to pure sandstone. The sample is square of side legth 5 cm. Correlation length CL is 0.05 cm.

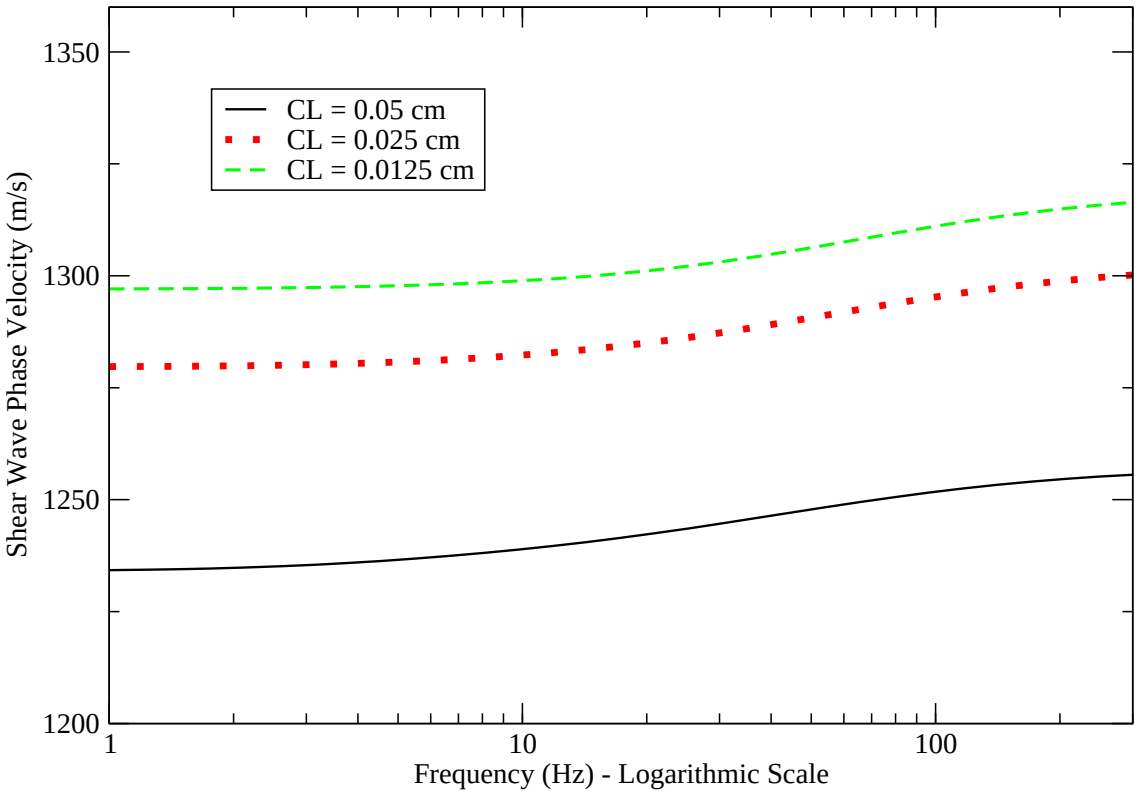

Fig. 15. Shear wave phase velocity as function of frequency for 50 % shale gas saturation for several correlation lengths CL. Residual saturations are $S_{rn} = 0, S_{rw} = 0.1$

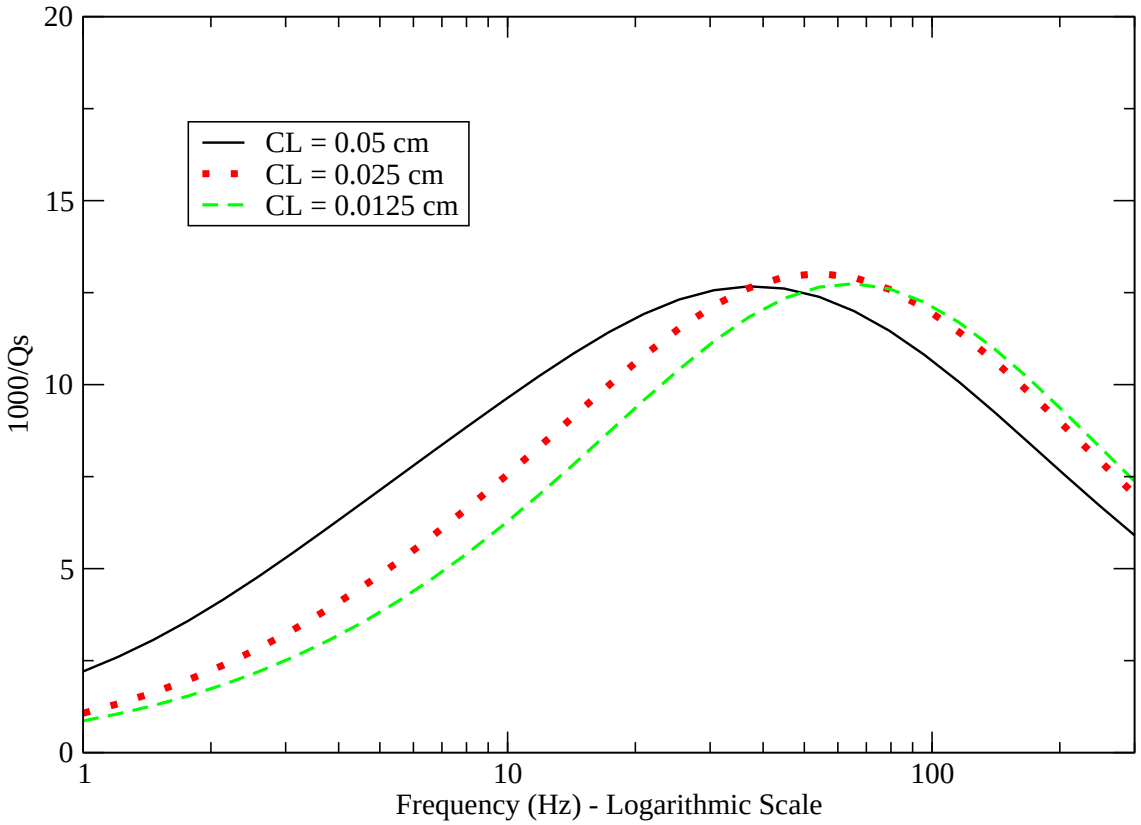

Fig. 16. Shear wave attenuation coefficient as function of frequency at 12 % gas saturation for several correlation lengths CL. Residual saturations are $S_{rn} = 0, S_{rw} = 0.1$